Self-Supervised Detection of Perfect and Partial Input-Dependent Symmetries

Alonso Urbano [1] **David W. Romero** [2 3]

Abstract

Group equivariance can overly constrain models if the symmetries in the group differ from those observed in data. While common methods address this by determining the appropriate level of symmetry at the dataset level, they are limited to supervised settings and ignore scenarios in which multiple levels of symmetry co-exist in the same dataset. In this paper, we propose a method able to detect the level of symmetry of each input without the need for labels. Our framework is general enough to accommodate different families of both continuous and discrete symmetry distributions, such as arbitrary unimodal, symmetric distributions and discrete groups. We validate the effectiveness of our approach on synthetic datasets with different per-class levels of symmetries, and demonstrate practical applications such as the detection of out-of-distribution symmetries. Our code is publicly available here.

1. Introduction

Symmetry transformations change certain aspects of the world state, e.g., shape, while maintaining others unaffected or invariant, e.g., class. Introducing inductive biases into the model architecture that reflect the underlying symmetries of the data has progressively become a key principle in the design of more efficient neural networks (Higgins et al., 2018). This is often achieved through the use of equivariance, a property that guarantees that a certain transformation made to the input of a neural network will result in a equivalent transformation in the corresponding output.

[1]Vrije Universiteit Amsterdam, Amsterdam, Netherlands [2]NVIDIA, Amsterdam, Netherlands [3]Work done while at the Vrije Universiteit Amsterdam. Correspondence to: Alonso Urbano <me@alonsourbano.com>, David W. Romero <dwromero@nvidia.com>.

Proceedings of the Geometry-grounded Representation Learning and Generative Modeling at 41st International Conference on Machine Learning, Vienna, Austria. PMLR Vol Number, 2024.
Copyright 2024 by the author(s).

Group equivariance leads to better generalization when the symmetries present in the data correspond to those in the group. However, if this is not the case, equivariance leads to overly constrained models and worse performance (Chen et al., 2020). To address this, common approaches involve manually adjusting the choice of the group to better reflect the symmetries in the data (Weiler & Cesa, 2019), or restricting the equivariance to subsets of the group. The latter is the case of Partial G-CNNs (Romero & Lohit, 2022), which implement partial equivariance layers and learn group subsets $\mathcal{S} \subseteq \mathcal{G}$ that best represents the symmetries in the data. This avoids overly constraining the model, as the equivariance is respected only for the learned levels of symmetry. Importantly, Partial G-CNNs learn this level of symmetry in a supervised manner and at a the dataset level, which means that they are unable to recognize unique, input-specific levels of symmetry. This poses a problem when different classes in the dataset exhibit varying symmetry levels (Fig. 1).

In this paper, we introduce a technique for learning levels of symmetry at a sample-level, without the need for labels. To achieve this, we build upon the Invariant-Equivariant Autoencoder (Winter et al., 2022), and infuse it with the ability to learn partial symmetries. As a result, we are able to predict the levels of symmetry of inputs during inference, and detect out-of-distribution symmetries. In addition, the properties of the network can be leveraged to reorient the inputs towards their centers of symmetry, allowing for generation of standardized datasets in which global symmetries are not present. In summary, our contributions are:

- We introduce a novel method to learn input-dependent levels of symmetries from data without the need for labels. Our method is able to determine both partial symmetries (subsets of the group) and perfect symmetries (spanning the entire group). We demonstrate that our framework is general enough to support a variety of symmetry distributions, such as arbitrary unimodal, symmetric distributions and discrete groups.

- We validate on synthetic datasets the efficiency of our method in predicting input-dependent symmetry levels. Additionally, we present practical applications, including the detection of out-of-distribution symmetries and the generation of symmetry-standardized datasets,

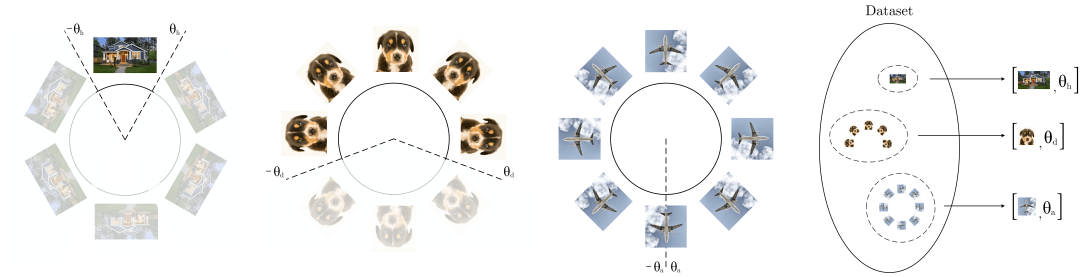

Figure 1. Self-supervised detection of input-dependent symmetries. In real world scenarios, different classes of objects present different levels of symmetries (*left*). Nevertheless, existing methods assume the same distribution of symmetries for all elements of the dataset. Our method can identify and determine the distribution of symmetries inherent to each input (*right*).

which can be leveraged to improve the performance of non-equivariant models.

2. Preliminaries

Our method builds upon Invariant-Equivariant Autoencoders (Winter et al., 2022) and it is motivated by Partial Group Equivariant CNNs (Romero & Lohit, 2022) ideas. In this section, we introduce these methods as well as the background concepts required for their understanding. The necessary basic definitions from group theory that back these methods can be found in Appendix A.

2.1. Invariant-Equivariant Autoencoder

Invariant-Equivariant Autoencoders (IE-AEs) (Winter et al., 2022) are able to generate a latent representation $(z, g) \in \mathcal{Z}=\{\mathcal{Z}_{\text{inv}}, \mathcal{Z}_{\text{equiv}}\}$ composed of an invariant $z \in \mathcal{Z}_{\text{inv}}$ and an equivariant component $g \in \mathcal{Z}_{\text{equiv}}$. The IE-AE is composed of two main parts: a $\mathcal{G}$-invariant autoencoder, and a $\mathcal{G}$-equivariant group action estimator.

$\mathcal{G}$-invariant autoencoder. The first component of the IE-AE is a $\mathcal{G}$-invariant autoencoder $\delta \circ \eta$ composed by a $\mathcal{G}$-invariant encoder η and a decoder δ. Its latent space $\mathcal{Z}_{\text{inv}}$ contains $\mathcal{G}$-invariant representations of the input. Note that, because η is $\mathcal{G}$-invariant, it holds that:

$$z = \eta(x) = \eta(\rho_{\mathcal{X}}(g)x) \in \mathcal{Z}_{\text{inv}}, \quad \forall g \in \mathcal{G}, \forall x \in \mathcal{X}. \tag{1}$$

That is, any $\mathcal{G}$-transformation of an input $x \in \mathcal{X}$ yields the same latent representation z in $\mathcal{Z}_{\text{inv}}$. Consequently, the decoder δ produces identical reconstructions $\hat{x}$ for every transformation the input:

$$\begin{aligned} \hat{x} = \delta(z) = \delta(\eta(x)) = \\ = \delta(\eta(\rho_{\mathcal{X}}(g)x)), \quad \forall g \in \mathcal{G}, \forall x \in \mathcal{X}. \end{aligned} \tag{2}$$

The $\mathcal{G}$-invariant reconstruction $\hat{x}$ corresponds to an element of the orbit of the input $\mathcal{O}_x$ i.e. $\hat{x} = \rho_{\mathcal{X}}(\hat{g}_x)x$ for some $\hat{g}_x \in \mathcal{G}$. This element $\hat{x}$ is denoted as the *canonical representation* of the decoder δ (or of the input x). As indicated by Winter et al. (2022), here "canonical" does not reflect any specific property of the element. It simply refers to the orientation $\rho_{\mathcal{X}}(\hat{g}_x)$ learned from the decoder during training, which may depend on various factors and hyperparameters. This is an important observation, as the central mathematical result of our work will concern the convenient collapse of this canonical representation via a constraint in the group action estimator.

Group action estimator. The other component of the architecture is the group action estimator $\psi : \mathcal{X} \to \mathcal{G}$. Recall that for a given input $x \in \mathcal{X}$, the canonical representation generated by the $\mathcal{G}$-invariant autoencoder is $\hat{x}=\delta(\eta(x))=\rho_{\mathcal{X}}(\hat{g}_x)x$, for some group element $\hat{g}_x$. The goal of ψ is to predict the transformation that maps the canonical representation $\delta(\eta(x))$ back to the original x. Therefore, such a function ψ must satisfy the property:

$$\rho_{\mathcal{X}}(\psi(x))\,\delta(\eta(x)) = x, \qquad \forall x \in \mathcal{X}. \tag{3}$$

A learnable function satisfying this property is denoted as a *suitable group action estimator*, and it can be constructed as $\psi = \xi \circ \mu$, where $\mu : \mathcal{X} \to \mathcal{Z}_{\text{equiv}}$ is a $\mathcal{G}$-equivariant network, and $\xi : \mathcal{Z}_{\text{equiv}} \to \mathcal{G}$ is a fixed deterministic function that maps the output of μ to a group element $g \in \mathcal{G}$.

Training the IE-AE. Winter et al. (2022) trains all the learnable components of the IE-AE (η, δ, ψ), jointly by optimizing the loss function:

$$\mathcal{L}_1 = d\left(\rho_{\mathcal{X}}(\psi(x))\,\delta(\eta(x)), x\right), \tag{4}$$

where d is a distortion metric, e.g., MSE. Note that Eq. 4 is group invariant by construction. This optimization loss leads to $\mathcal{G}$-invariant representations of the input in the latent space $\mathcal{Z}_{\text{inv}}$, and a $\mathcal{G}$-equivariant estimation $g \in \mathcal{Z}_{\text{equiv}}$ of the transformation needed to reorient $\hat{x}$.

Unlike IE-AEs, our method is not limited to perfect symmetries, and generates consistent, meaningful canonical representations for semantically similar data-points: an ability IE-AEs lacks (Fig. 3).

2.2. Partial Group Equivariant Convolutional Neural Networks

A map $h : \mathcal{V} \to \mathcal{W}$ is said to be partially equivariant to $\mathcal{G}$ with respect to the representations $\rho_{\mathcal{V}}, \rho_{\mathcal{W}}$ if it is equivariant

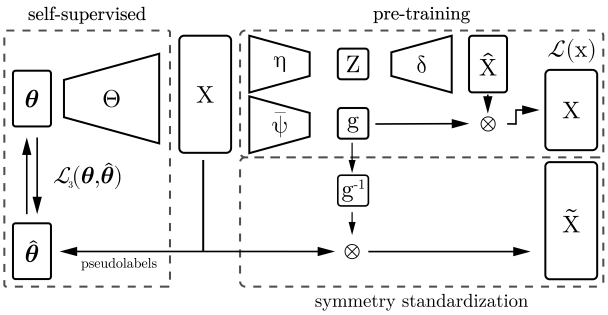

Figure 2. Overview of our proposed method.

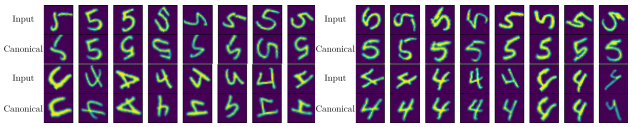

Figure 3. Canonical orientations obtained during inference by the IE-AE (Winter et al., 2022) *(left)* and our method *(right)*. Both models are trained on MNISTRot60-90, a dataset exhibiting uniform rotational symmetries within $[-60°, 60°]$ for digits 0 to 4 and $[-90°, 90°]$ for digits 5 to 9. Our method is able to consistently choose the center of each input's symmetry distribution as the canonical representation (Prop. 3.1 *(ii)*).

only to transformations on a *subset* $\mathcal{S}$ of the group $\mathcal{G}$. That is, if $h(\rho_{\mathcal{V}}(g)x) = \rho_{\mathcal{W}}(g)h(x)$, $\forall g \in \mathcal{S} \subseteq \mathcal{G}, \forall x \in \mathcal{X}$ (Romero & Lohit, 2022).[1] Partial G-CNNs can be seen as G-CNNs able to relax their equivariance constraints to hold only on subsets $\mathcal{S} \subseteq \mathcal{G}$ based on the training data. Partial G-CNNs adaptively learn the subsets $\mathcal{S}$ from data by defining a probability distribution on the group from which group elements are sampled during the forward pass at each layer, and learning their parameters during training. In the context of continuous groups, Partial G-CNNs learn connected subsets of group elements $\mathcal{S}=\{\theta^{-1}, ..., e, ..., \theta\} \subseteq \mathcal{G}$ by defining a uniform distribution $\mathcal{U}[-\theta, \theta]$ on the group and learning the value of θ with the reparameterization trick (Kingma & Welling, 2013; Falorsi et al., 2019). By doing so, Partial G-CNNs are able to fine-tune their equivariance to match the symmetries observed in data, resulting in models with more flexible equivariance constraints than G-CNNs.

It is worth noting that Partial G-CNNs identify partial symmetries at a *dataset level*, whereas our method identifies different symmetry levels for individual dataset elements, without relying on partial convolutions. In addition, our method generalizes beyond uniform distributions. Here, we demonstrate its extension to arbitrary unimodal, symmetric distributions as well as discrete groups.

3. Self-Supervised Detection of Perfect and Partial Input-Dependent Symmetries

We aim to learn, without the need for labels, the input-dependent symmetry subsets of the group that accurately represent the symmetries appearing in the data. Similarly to Romero & Lohit (2022), we achieve this by learning a probability distribution $\mathrm{p}(u)$ on the group such that $\mathrm{p}(u)$ is zero for transformations that do not appear in the data. Focusing on the continuous group of planar rotations $\mathcal{G}$=SO(2), we consider a uniform distribution $\mathcal{U}[-\theta, \theta]$ defined over a connected set of group elements $\{g_{-\theta}, ..., e, ..., g_{\theta}\}$. This translates into learning the θ parameter of the distribution, which we refer to as the *symmetry boundary*. Assuming that datasets can have different symmetry boundaries per sample, this implies that we aim to learn a family of distributions $\mathcal{F}=\{\mathcal{U}[-\theta_x, \theta_x]\}_{x\in\mathcal{X}}$, where the symmetry boundary θ_x depends on the input x.

The proposed method is detailed in Fig. 2. First, we train a modified IE-AE, constrained to encourage meaningful canonical representations across semantically similar inputs (Sec. 3.2), to capture the distribution of symmetries of data. We term this the *pre-training* phase. Next, we use the learned distribution to estimate input-dependent symmetry boundaries, which are then used as pseudo-labels for the self-supervised training of the network Θ. Θ is ultimately responsible for the prediction of the level of symmetry of the input (Sec. 3.4). We term this the *self-supervision* phase. After training, the IE-AE can be discarded and the Θ network alone can be used to predict the symmetry level of an input during inference. In addition, we can leverage the inferred canonical representations to transform the original dataset into one in which these symmetries are not present. We term this *symmetry standardization* (Sec. 3.5).

3.1. Learning input-depending symmetries from data

Consider the equivalence relation $\sim_{\mathcal{G}}$ in $\mathcal{X}$ defined by $x \sim_{\mathcal{G}} y$ if and only if $\exists g \in \mathcal{G}$ such that $x=\rho_{\mathcal{X}}(g)y$, and the corresponding quotient set $\mathcal{X}/\sim_{\mathcal{G}}$. Under this definition, two elements of the dataset are related by $\sim_{\mathcal{G}}$ if and only if they are equal up to a $\mathcal{G}$-transformation. Therefore, the equivalence classes $[x] \in \mathcal{X}/\sim_{\mathcal{G}}$ contain the information about the symmetries of each input $x \in \mathcal{X}$.

We assume that the rotation symmetries of every input $x \in \mathcal{X}$ are uniformly distributed in $[-\theta_x, \theta_x]$ for a symmetry boundary (or level of symmetry) θ_x that depends on x. We refer to this assumption as *uniformity of symmetries*. Then, every class $[x] \in \mathcal{X}/\sim_{\mathcal{G}}$ has a unique element $c_{[x]} \in [x]$ that is the center of the uniform symmetry, which corresponds to a rotation by zero degrees in the interval $[-\theta_x, \theta_x]$. Note that under the presented framework, the symmetry boundary angle depends on the equivalence class of the input rather than on the input itself, i.e. $\theta_x=\theta_{[x]}$. This is because, as

[1] As noted in Romero & Lohit (2022), partial equivariance is in general only approximate because $\mathcal{S}$ is not necessarily closed under $\cdot$. If $\mathcal{S}$ is closed under $\cdot$, then it forms a *subgroup* of $\mathcal{G}$, and $\mathcal{S}$-equivariance is exact.

per the definition of $\sim_{\mathcal{G}}$, all elements of a given equivalence class share the same orbit.

With this insight in mind, we can write the elements s of a class $[x]$ as $s{=}\rho_{\mathcal{X}}(g)c_{[x]}$ for group elements g in $\mathcal{S}_{\theta_{[x]}}$, which is defined as the subset of G with rotation angles in the interval $[-\theta_{[x]}, \theta_{[x]}]$. For instance, in a dataset in which every input has rotational symmetries in $[-60°, 60°]$, the set $\mathcal{S}_{\theta_{[x]}}$ would consist of all the elements of SO(2) with rotation angle in $[-60°, 60°]$. Lastly, let us denote $\psi([x])$ as the images of the elements of $[x]$ obtained by the group action estimator ψ. Note that if the rotations in $\psi([x])$ correspond to the rotations in the distribution $\mathcal{U}[-\theta_{[x]}, \theta_{[x]}]$ for each $[x] \in \mathcal{X}/\sim_{\mathcal{G}}$, then ψ is predicting precisely the symmetries appearing in the data. Following the previous example, the equality $\psi([x]) = \mathcal{S}_{\theta_{[x]}}$ would mean that the predictions of ψ for each class are rotations with angles in $[-60°, 60°]$. We are now ready to state the following proposition:

Proposition 3.1. *Consider a $\mathcal{G}$-invariant autoencoder $\delta \circ \eta$ and a group action estimator ψ. Under the assumption of uniformity of symmetries in $\mathcal{X}$, the following statements are equivalent:*

(i) $\psi\left(c_{[x]}\right) = e \;\forall [x] \in \mathcal{X}/\sim_{\mathcal{G}}$.

(ii) $\forall [x] \in \mathcal{X}/\sim_{\mathcal{G}}$, *the canonical representation of any* $s \in [x]$ *is its center of symmetry* $c_{[x]}$.

(iii) $\forall [x] \in \mathcal{X}/\sim_{\mathcal{G}}$, *it holds that* $\psi([x]) = \mathcal{S}_{\theta_{[x]}}$.

Proof. See Appendix B. □

The proposition states that, under the constraint introduced in *(i)*, conditions *(ii)* and *(iii)* are satisfied. This implies that a group action estimator constrained by *(i)*, which we denote as $\bar{\psi}$, can effectively collapse the canonical representation of an input into the center of symmetry of its equivalence class, thereby validating its canonical status. Moreover, it ensures that the choice of the canonical representation is consistent across inputs sharing the same invariant representation. This intra-class consistency with meaningful canonical representations is not guaranteed in IE-AEs, as shown in Fig. 3.

Condition *(iii)* states that the symmetries of the class $[x]$, given by $\mathcal{S}_{\theta_{[x]}}$, can be obtained by calculating the image of $[x]$ by ψ. This means that, under this constraint, the group action estimator effectively learns the input-dependent distribution of symmetries in the data, unlike in IE-AEs, whose distribution fails to align with the data's inherent symmetries (Fig. 4). In summary, Prop. 3.1 establishes that the constraint in Prop. *(i)* serves as a sufficient and necessary condition to learn subsets of symmetries in the data, and achieve consistent, meaningful canonical representations.

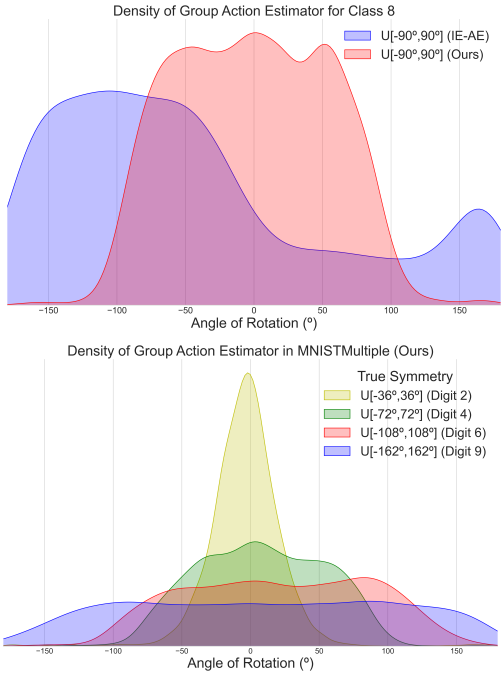

Figure 4. Distribution of the transformations predicted by ψ with the IE-AE and our method in class 8 from MNISTRot60-90 *(top)*. Our group action estimator $\bar{\psi}$ correctly captures the different input-dependent distributions in the dataset by means of the constraint in Proposition 3.1 *(i) (bottom)*.

3.2. Learning constrained group action estimators

In practice, it is not possible to apply the constraint $\psi(c_{[x]}){=}e \;\forall [x] \in \mathcal{X}/\sim_{\mathcal{G}}$ to the group action estimator, as we do not know a priori which elements in the dataset are centers of symmetry. However, we can encourage convergence to this solution by minimizing $d\left(\psi(x), e\right)$, with d a distorsion metric, e.g., MSE (see Appendix B.1). Combining this term with the loss term of Eq. 4, we obtain an optimization loss:

$$\begin{aligned}\mathcal{L} &= \mathcal{L}_1 + \mathcal{L}_2 = \\ &= d_1\left(\rho_{\mathcal{X}}(\psi(x))\,\delta(\eta(x)), x\right) + d_2\left(\psi(x), e\right).\end{aligned} \tag{5}$$

Jointly optimizing $\mathcal{L}_1$ and $\mathcal{L}_2$ encourages convergence to solutions that comply with Proposition 3.1.

3.3. Estimation of the symmetry boundary

Suppose we have pre-trained our constrained group action estimator using the loss $\mathcal{L}$ as per Eq. 5. Prop. 3.1 *(iii)* states that the symmetry distribution of an input x is defined by the image of its equivalence class $[x]$ under ψ. However, calculating these equivalence classes is infeasible in practice, since $\mathrm{SO}(2)$ is an infinite group. To overcome this problem, we base our approach on the convenient assumption that *similar objects share the same distribution of symmetries*. This assumption is grounded in empirical observations across diverse real-world scenarios in which different objects within

the same class exhibit consistent symmetrical patterns, such as a shared rotational distribution. In essence, we argue that inputs semantically similar to x contain information about the symmetries of x, much like its equivalence class $[x]$. Section 5 contains a practical discussion of this assumption and its trade-offs.

Motivated by this observation, we shift from using equivalence classes $[x]$ to sets of objects semantically similar to x for estimating its level of symmetry θ_x. This approach bypasses the need for calculating equivalence classes, and allows for a self-supervised learning of θ_x through the use of estimations of θ_x in the form of pseudo-labels.

3.4. Self-supervised learning of the symmetry boundaries

Generating the pseudo-labels. Let $\mathcal{N}_{k,d}{=}\mathcal{N}_k : \mathcal{X} \to \mathcal{P}(\mathcal{X})$ be a function that maps each input x to the set $\mathcal{N}_{k,d}(x) \subset \mathcal{X}$ of k-neighbors around x in the $\mathcal{G}$-invariant latent space $\mathcal{Z}_{\text{inv}}$ as measured by some distance metric d, i.e., the k elements of the dataset whose $\mathcal{G}$-invariant embeddings are closest to the $\mathcal{G}$-invariant embedding of x, $\eta(x)$. $\mathcal{N}_k(x)$ acts as a substitute of the equivalence class $[x]$, and contains elements semantically similar to x, which we assume to share the symmetry distribution of x. We then estimate the level of symmetry of x within the dataset $\mathcal{X}$ by estimating the parameter of the distribution corresponding to $\psi(\mathcal{N}_k(x))$ with an estimator E of uniform distributions of the form $\mathcal{U}[-\theta, \theta]$. In practice, we found beneficial to convert the original distribution $\mathcal{U}[-\theta, \theta]$ to a distribution $\mathcal{U}[0, \theta]$ by taking the absolute value of ψ's predictions. We then use the Method of Moments estimator for uniform distributions of this form, which proved to be more robust to outliers than other estimators, resulting in more reliable pseudo-labels (Appx. C). Combining all components, we calculate the pseudo-labels $\hat{\theta}_x$ that estimate the symmetry boundary θ_x as:

$$\hat{\theta}_x = (E \circ |\psi| \circ \mathcal{N}_k)(x) \tag{6}$$

Learning the levels of symmetry. Once we calculate the pseudo-labels, we can use them to learn the levels of symmetry of each input $x \in \mathcal{X}$ in a self-supervised manner. To this end, we introduce a *boundary prediction network* $\Theta = \omega \circ \phi : \mathcal{X} \to \mathbb{R}^+$ consisting of a $\mathcal{G}$-invariant network ϕ, followed by a fully connected network ω. The boundary prediction network Θ is trained to minimize the difference between the predicted symmetry boundary $\Theta(x)$, and the estimated pseudo-label $\hat{\theta}_x$:

$$\mathcal{L}_3 = d\left(\Theta(x), \hat{\theta}_x\right). \tag{7}$$

The $\mathcal{G}$-invariance in Θ reflects that all samples on an orbit share the same level of symmetry $\theta_{[x]}$.

3.5. Symmetry standardization

Our method also allows for the removal of symmetries in a given dataset based on its symmetric properties. Prop. 3.1 states that, under the constraint outlined in Prop. 3.1 *(i)*, the canonical representation of every element $x \in [x]$ is the center of symmetry $c_{[x]}$ for all $[x] \in \mathcal{X}/{\sim_{\mathcal{G}}}$. Let $\overline{\psi}$ denote a group action estimator subject to this constraint. Recall that any $x \in \mathcal{X}$ belongs to an equivalence class $[x]$ with a unique center of symmetry $c_{[x]}$. Since $\overline{\psi}$ is suitable, then:

$$\begin{aligned} x &= \rho_{\mathcal{X}}(\overline{\psi}(x))\delta(\eta(x)) = \rho_{\mathcal{X}}(\overline{\psi}(x))\hat{x} \overset{\text{Prop. 3.1 (ii)}}{=} \\ &\rho_{\mathcal{X}}(\overline{\psi}(x))c_{[x]} \iff \rho_{\mathcal{X}}(\overline{\psi}(x)^{-1})x = c_{[x]}. \end{aligned} \tag{8}$$

That is, the inverse of the group actions predicted by $\overline{\psi}$ can be used to reorient the input towards the center of symmetry of its class. This can be done efficiently for every input without involving the calculation of the classes $[x]$. Then, the set $\tilde{\mathcal{X}} = \left\{\rho_{\mathcal{X}}(\overline{\psi}(x)^{-1})x\right\}_{x \in \mathcal{X}}$, is a standardized, $\mathcal{G}$-invariant version of the data $\mathcal{X}$ whose symmetries have been effectively removed by collapsing every input into the orientation of the center of symmetry of its class.

3.6. Considering other groups and symmetry distributions

Our method is not restricted to uniform symmetry distributions. It can consider other symmetry distributions –both continuous and discrete– by adjusting the hypotheses in Proposition 3.1, and deriving appropriate estimators for the pseudo-labels. Furthermore, we show that, for arbitrary unimodal, symmetric distributions, the objective $\mathcal{L}_2$ converges to the center of symmetry $c_{[x]}$, allowing us to learn and predict symmetry levels through the previous construction (Appx. B.1).

Gaussian symmetries. Consider a dataset $\mathcal{X}$, whose elements are governed by rotational symmetries $\mathcal{S}_{\sigma_{[x]}} \subset \mathcal{G}$ sampled from a Gaussian distributions $N(0, \sigma_{[x]})$, whose center is defined as the center of symmetry $c_{[x]}$. Under these assumptions, the following proposition holds:

Proposition 3.2. *Consider a $\mathcal{G}$-invariant autoencoder $\delta \circ \eta$ and a group action estimator ψ. Under Gaussian symmetries in $\mathcal{X}$, the following statements are equivalent:*

(i) $\psi\left(c_{[x]}\right) = e \ \forall [x] \in \mathcal{X}/{\sim_{\mathcal{G}}}$.

(ii) $\forall [x] \in \mathcal{X}/{\sim_{\mathcal{G}}}$, *the canonical representation of any* $s \in [x]$ *is its center of symmetry* $c_{[x]}$.

(iii) $\forall [x] \in \mathcal{X}/{\sim_{\mathcal{G}}}$, *it holds that* $\psi([x]) = \mathcal{S}_{\sigma_{[x]}}$.

Proof. See Appendix B. □

Discrete symmetries. We can also consider datasets governed by discrete symmetric groups, e.g., the cyclic order n subgroups of $\mathrm{SO}(2)$, $\mathcal{C}_n$. In this case, each dataset sample

x shows cyclic symmetries given by a group $\mathcal{S}_{n_{[x]}}$=$\mathcal{C}_{n_{[x]}}$ of order $n_{[x]} \in \mathbb{N}$. Importantly, note that since cyclic groups are intrinsically symmetric, *every element of* $\mathcal{S}_{n_{[x]}}$ *is equally valid to serve as center of symmetry*. This property of symmetric discrete groups lets us relax the condition (i) in Proposition 3.3:

Proposition 3.3. *Consider a* $\mathcal{G}$*-invariant autoencoder* $\delta \circ \eta$ *and a group action estimator* ψ*. Under cyclic symmetries in* $\mathcal{X}$*, the following statements are equivalent:*

(i) $\psi\left(c_{[x]}\right)$=e $\forall [x] \in \mathcal{X}/\sim_{\mathcal{G}}$ *for some* $c_{[x]} \in [x]$.

(ii) $\forall [x] \in \mathcal{X}/\sim_{\mathcal{G}}$*, the canonical representation of any* $s \in [x]$ *is the element* $c_{[x]} \in [x]$.

(iii) $\forall [x] \in \mathcal{X}/\sim_{\mathcal{G}}$*, it holds that* $\psi\left([x]\right) = \mathcal{C}_{n_{[x]}}$.

Proof. See Appendix B. □

As shown in Appx. C, we can construct proper group action estimators for each of these symmetry distributions in order to generate appropriate pseudo-labels for Θ.

Other groups. In general, our framework applies to arbitrary groups, given that a method for the estimation of the symmetry distribution parameter via the neighbors is provided. We provide proofs for cyclic groups $\mathcal{C}_n$ and distributions in $\mathrm{SO}(2)$, but it can be shown that e.g. the group of reflections around a fixed axis in the 2D case (or around a fixed plane in the 3D case) also apply. For instance, by realizing that both these groups are isomorphic to $\mathcal{C}_2$. In this work, we empirically demonstrate our method for uniform and Gaussian distributions over $\mathrm{SO}(2)$ and for cyclic groups.

4. Related work

Unsupervised learning of invariant and equivariant representations. Unsupervised learning of both invariant and equivariant representations through the use of autoencoder-based approaches has been previously proposed (Shu et al., 2018; Guo et al., 2019; Feige, 2019; Kosiorek et al., 2019; Koneripalli et al., 2020; Winter et al., 2021; 2022; Yokota & Hontani, 2022). However, existing methods, e.g., Quotient Autoencoders (QAE) (Yokota & Hontani, 2022), Invariant-Equivariant Autoencoders (Winter et al., 2022) obtain arbitrary preferred orientations –or canonical representations. In contrast to existing approaches, our proposed work is not limited to perfect symmetries, and is able to learn meaningful consistent canonical representations.

Soft equivariance and soft invariance. Typical group equivariant approaches do not inherently learn their level of symmetry based on data. Instead, these symmetries are imposed manually through the choice of the group prior to training (Cohen & Welling, 2016; Cohen et al., 2018; Weiler et al., 2018; Weiler & Cesa, 2019; Cohen et al., 2019; Romero et al., 2020; Romero & Cordonnier, 2020; Wang et al., 2020). This approach has limitations when dealing with datasets that contain partial symmetries –such as real-world images– resulting in overly constrained models. In such cases, *soft* or *partial* equivariance (or invariance) is desired, allowing these properties to hold only for a subset of the group transformations. Canonical examples are Augerino (Benton et al., 2020) and Partial G-CNNs (Romero & Lohit, 2022), which achieve this by learning a probability distribution over transformations. Other approaches handle soft equivariance through a combination of equivariant and non-equivariant models (Finzi et al., 2021a;b). Nevertheless, existing approaches generally require supervised training, and only capture levels of symmetry at a dataset-level. In contrast, our method is able to learn levels of symmetry at a sample-level, and does so in a self-supervised manner.

Symmetry standardization. Finally, Spatial Transformer Networks (STN) (Jaderberg et al., 2015) transform the input to counteract data transformations through a learnable projective operation. This is similar to our data standardization process. However, STNs are usually trained in a supervised manner, as part of a broader network for tasks like classification. Instead, we produce symmetry standardization without relying on labelled examples.

5. Experiments

In this section, we evaluate our approach. Comprehensive implementation details, including architecture specifications and optimization techniques, can be found in Appx. D.

Prediction of input-dependent levels of symmetry. To evaluate the ability of our method to predict the levels of symmetry, we use standard and synthetic versions of the MNIST-12K (LeCun et al., 1998) dataset, divided into $12,000$ train and $50,000$ test images, as well as the FashionMNIST (Xiao et al., 2017) dataset, divided into $50,000$ train and $10,000$ test images. We construct RotMNIST60, an MNIST variation with digits uniformly rotated in the interval $[-60°, 60°]$; RotMNIST60-90, a variation with digits uniformly rotated in $[-60°, 60°]$ for the classes 0–4, and in $[-90°, 90°]$ for the classes 5–9; and MNISTMultiple, a MNIST variation with different rotational symmetries per class starting from zero rotation for the class 0, and increasing the maximum rotation by $18°$ in each class, i.e., $[-18°, 18°]$ for class 1, $[-36°, 36°]$ for class 2, etc. Similarly, we create FashionMNIST variants for the 60-90 and multiple symmetries case (Fashion60-90, FashionMultiple). We also create a Gaussian variation of MNISTMultiple: MNISTGaussian, which exhibits rotational Gaussian distributions with increasing standard deviations per-class, following multiples of $9°$. This choice ensures that 95% of sampled rotations falls within the corresponding MNISTMultiple's interval. For the cyclic case, we construct MNISTC2-C4, an analogous to MNISTRot60-90 where rotations are

Table 1. Comparison of test set accuracy scores of baseline supervised and unsupervised models (ResNet-18 and K-Means respectively), with and without the use of symmetry standardization.

Dataset	ResNet-18		K-Means		IE-AE + KNN
	Regular	Symmetry Std.	Regular	Symmetry Std.	
MNISTRot60	**97.47%**	97.39%	65.58%	**86.81%**	95.58%
MNISTRot60-90	96.99%	**97.23%**	64.74%	**86.36%**	95.31%
MNISTMultiple	96.79%	**97.16%**	61.93%	**86.22%**	95.80%
MNISTGaussian	**96.70%**	96.58%	65.00%	**86.06%**	95.65%
MNISTC2-C4	97.23%	**97.53%**	66.01%	**81.83%**	95.22%
MNISTRot	95.39%	**96.35%**	42.70%	**83.61%**	95.25%
Fashion60-90	86.49%	**89.07%**	58.17%	**67.96%**	83.43%
FashionMultiple	90.08%	**90.92%**	63.39%	**69.55%**	84.68%

Table 2. Test accuracy for out-of-distribution symmetry detection.

	Accuracy
RotMNIST	92.27%
RotMNIST60-90	91.30%
MNISTMultiple	86.48%
MNISTGaussian	83.64%
MNISTC2-C4	82.47%
Fashion60-90	88.67%
FashionMultiple	81.88%

drawn from C_2 and C_4 for the corresponding class subsets. We additionally evaluate our method on the standard MNIST and rotated MNIST (RotMNIST Larochelle et al. (2007)).

We consider two metrics in our evaluation: the average predicted symmetry level $\overline{\Theta}$, and the Mean Absolute Error (MAE) between the predictions and the true boundary angles θ. All metrics are calculated in the test set, and the best model is chosen based on best loss obtained during validation. Our results are summarized in Fig. 5 and shown in an extended format in Tabs. 3, 4 5, 6.

For datasets with full rotational symmetries (MNISTRot) and no symmetries (MNIST-12K), our method obtains consistently accurate predictions of the symmetry levels across all classes. For MNIST-12K, we note minor deviations from the expected symmetry level of $0°$ across all classes. Rather than an imprecision, we attribute this to the inherent rotational symmetries proper of handwritten digits caused by diverse writing styles and nuances.

In datasets with partial symmetries, our model consistently identifies the correct level of symmetry across all classes. This is true even when various levels of symmetry are present within a single dataset. For instance, the MNISTRot60 experiment highlights our model's ability to adapt to partial symmetries, while results from the MNISTRot60-90 experiment show its capability to discern varying levels of symmetry on a per-class basis. In the challenging MNISTMultiple dataset, our model consistently predicts varying symmetry levels for each class, showcasing its ability to handle diverse, intricate symmetry scenarios. Furthermore, results on MNISTGaussian show that our method generalizes to other unimodal, symmetric distributions, even in scenarios with different symmetry distributions per-class.

We observe a similar performance on the FashionMNIST variants, with moderate deviations from the true symmetry level for class 8 in Fashion60-90 and class 6 in FashionMultiple. This deviation in class 6 (shirt) can be linked to the underlying assumption discussed in Section 3.3, where we assume that similar objects share the same distribution of symmetries. In the invariant latent space, shirts (class 6) and t-shirts (class 0) are very close to each other – perhaps even overlapping. Hence, the deviation arises because the neighbors selected for the shirt class likely included some t-shirts (class 0), which have a true symmetry of $0°$, thus skewing the estimated symmetry level for the shirts.

Note that our method exercises the assumption by selecting a relatively small number of neighbors (45 neighbors, as detailed in Appendix D) around each input, effectively managing its range. This allows our method to infer different symmetry levels even for inputs that seemingly violate the assumption, as we can observe for shirts and t-shirts which show more than $60°$ difference in their predicted symmetry level. Additionally, this approach tends to perform better as the dataset grows in size, since a denser latent space enhances the similarity of neighboring data points.

On MNISTC2-C4 we observe that our model presents some inaccuracies for the classes 3, 4, and 5. However, looking at the per-class density estimations (Fig. 6, Appx. D) confirms that ψ accurately captures data symmetries as outlined in Prop.3.3. The observed imprecision stems likely from the limitations of our density-comparison approach for generating pseudo-labels, which is error-prone due to requiring very high number of neighbours per-input. Implementing more sophisticated methods to estimate cyclic groups from densities could enhance the precision of these estimations.

Out-of-distribution (OOD) symmetry detection. We further validate our method for the detection of objects whose symmetries differ from those observed during training. To this end, randomly rotated inputs are passed through a classifier, whose task is to predict whether the input's symmetries

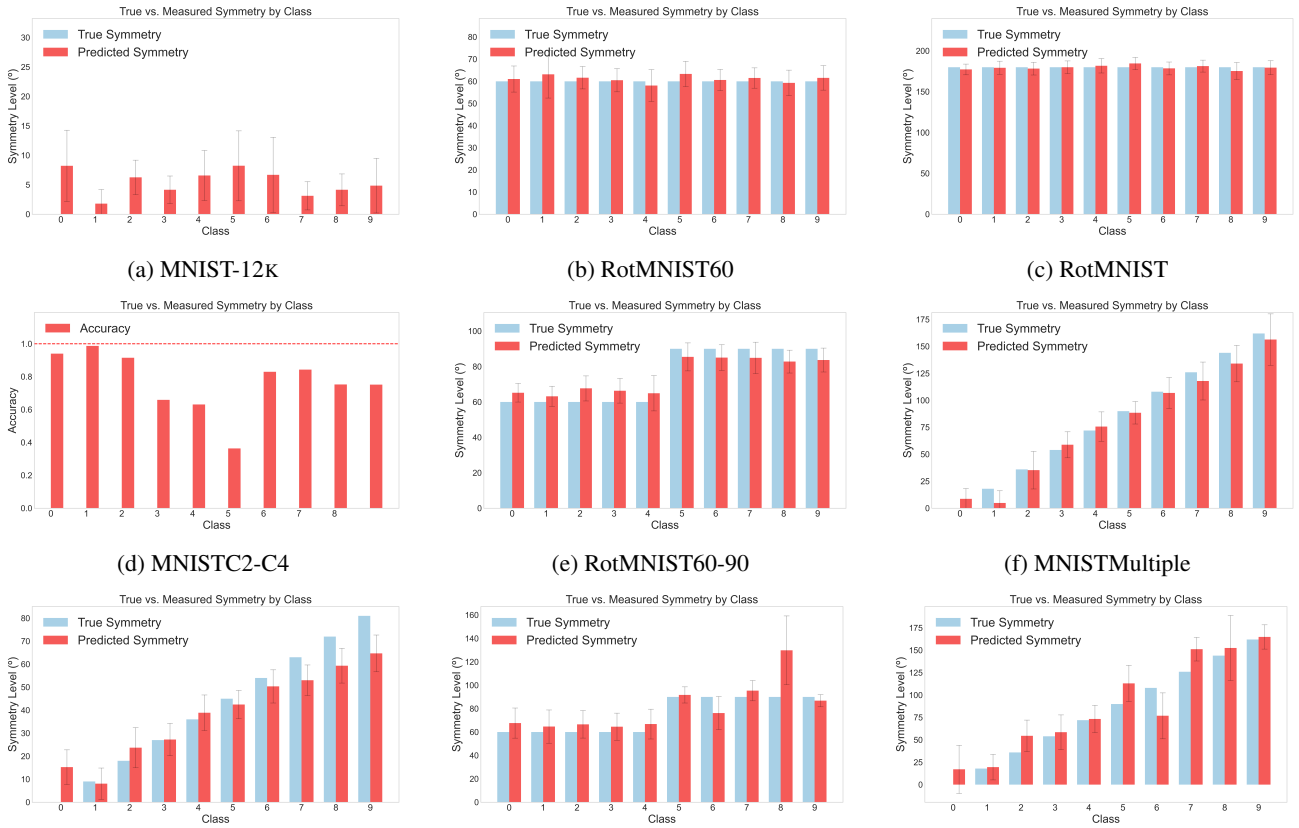

(a) MNIST-12K (b) RotMNIST60 (c) RotMNIST

(d) MNISTC2-C4 (e) RotMNIST60-90 (f) MNISTMultiple

(g) MNISTGaussian (h) Fashion60-90 (i) FashionMultiple

Figure 5. Prediction of input-dependent levels of symmetry on rotation augmented variants of MNIST and FashionMNIST.

has been seen during training or not. These OOD classifiers use the boundary prediction network Θ trained on the previous section, and are tested on fully-rotated unseen inputs without further training (see Appx. D.2).

As shown in Table 2, all models consistently demonstrate their ability to identify unseen symmetries during inference. As expected, there is a modest decline in the performance of the out-of-distribution detection models as the complexity of the symmetries in the data increases. Nevertheless, even in datasets with intricate and multiple symmetries, we achieve high OOD prediction accuracies (e.g. 86.48% for MNIST-Multiple and 88.67% on Fashion60-90), which underscores the potential for practical applications of our method.

Improving non-equivariant models with symmetry standardization. To conclude, we investigate the impact of symmetry standardization in the performance of non-equivariant models. To achieve this, we consider baseline supervised and unsupervised learning models: ResNet-18 (He et al., 2015) and K-Means, and compare the performances obtained with the original datasets against those obtained using the symmetry-standardized versions generated by our method. As shown in Tab. 1, both unsupervised and supervised methods see performance enhancements from symmetry standardization, specially for K-Means.

To further evaluate the advantages of symmetry standardization, we compare it with a supervised K-Nearest Neighbors (KNN) classifier trained on the $\mathcal{G}$-invariant embeddings of an IE-AE (Tab. 1), as done in Winter et al. (2022). While IE-AE embeddings offer improvements thanks to their $\mathcal{G}$-invariance, they can only be used as embeddings for other models as in the KNN case. In contrast, symmetry standardization transfers the $\mathcal{G}$-invariance to the data itself, allowing other methods to operate directly on the $\mathcal{G}$-invariant data without being constrained to use the low-dimensional embeddings of an IE-AE. It is worth noting that, in principle, symmetry standardization could also be achieved with regular IE-AEs. However, it is essential to have *consistent, meaningful canonical representations to collapse to during this process* –a property that IE-AEs lack (Fig. 3). We achieve this through the constraint proposed in Proposition 3.1*(i)*.

6. Conclusions and limitations

We proposed a method to determine the distribution of symmetries for each input in the dataset in a self-supervised manner. We showed through various experiments the effectiveness of our method, showcasing its ability to adapt

to multiple, complex symmetries –both perfect and partial– within a same dataset. Furthermore, our method is able to accommodate different families of symmetry distributions and groups, and offers practical benefits, notably in out-of-distribution symmetry detection.

Limitations. The main limitation of our method is related to the symmetry distributions it is able to represent. Specifically, the main assumption for finding $c_{[x]}$ is that the underlying symmetry distribution is both unimodal and symmetric. Extending our results to complex, multimodal symmetry distributions is an interesting direction for future research. In addition, our method is limited by the group actions that can be represented by an IE-AE. We observe that in datasets with high intra-class variability, e.g., CIFAR10, objects within the same class may not share a $\mathcal{G}$-invariant representation that connects them through a group action. In such cases, the MSE loss of IE-AEs is unable to capture this relationship (Eq. 4), limiting our method. In the future, we aim to mitigate this through the use of more semantically meaningful metrics such as SSIM (Wang et al., 2004).

Acknowledgments

This work was partially carried out on the Dutch national infrastructure with the support of SURF Cooperative. We used Weights & Biases (Biewald, 2020) for experiment tracking and visualizations.

We thank Carlos Saavedra Luque for his valuable contribution to the design of several figures presented in this paper.

References

Benton, G. W., Finzi, M., Izmailov, P., and Wilson, A. G. Learning invariances in neural networks. *CoRR*, abs/2010.11882, 2020. URL https://arxiv.org/abs/2010.11882.

Biewald, L. Experiment tracking with weights and biases, 2020. URL https://www.wandb.com/. Software available from wandb.com.

Chen, S., Dobriban, E., and Lee, J. H. A group-theoretic framework for data augmentation. *Journal of Machine Learning Research*, 21(245):1–71, 2020.

Cohen, T. and Welling, M. Group equivariant convolutional networks. In *International conference on machine learning*, pp. 2990–2999. PMLR, 2016.

Cohen, T., Geiger, M., and Weiler, M. A general theory of equivariant cnns on homogeneous spaces. *CoRR*, abs/1811.02017, 2018. URL http://arxiv.org/abs/1811.02017.

Cohen, T. S., Weiler, M., Kicanaoglu, B., and Welling, M. Gauge equivariant convolutional networks and the icosahedral CNN. *CoRR*, abs/1902.04615, 2019. URL http://arxiv.org/abs/1902.04615.

Falorsi, L., de Haan, P., Davidson, T. R., and Forré, P. Reparameterizing distributions on lie groups. In *The 22nd International Conference on Artificial Intelligence and Statistics*, pp. 3244–3253. PMLR, 2019.

Feige, I. Invariant-equivariant representation learning for multi-class data, 2019.

Finzi, M., Benton, G. W., and Wilson, A. G. Residual pathway priors for soft equivariance constraints. *CoRR*, abs/2112.01388, 2021a. URL https://arxiv.org/abs/2112.01388.

Finzi, M., Welling, M., and Wilson, A. G. A practical method for constructing equivariant multilayer perceptrons for arbitrary matrix groups. *CoRR*, abs/2104.09459, 2021b. URL https://arxiv.org/abs/2104.09459.

Guo, X., Zhu, E., Liu, X., and Yin, J. Affine equivariant autoencoder. In *Proceedings of the Twenty-Eighth International Joint Conference on Artificial Intelligence, IJCAI-19*, pp. 2413–2419. International Joint Conferences on Artificial Intelligence Organization, 7 2019. doi: 10.24963/ijcai.2019/335. URL https://doi.org/10.24963/ijcai.2019/335.

He, K., Zhang, X., Ren, S., and Sun, J. Deep residual learning for image recognition. *CoRR*, abs/1512.03385, 2015. URL http://arxiv.org/abs/1512.03385.

Higgins, I., Amos, D., Pfau, D., Racanière, S., Matthey, L., Rezende, D. J., and Lerchner, A. Towards a definition of disentangled representations. *CoRR*, abs/1812.02230, 2018. URL http://arxiv.org/abs/1812.02230.

Jaderberg, M., Simonyan, K., Zisserman, A., and Kavukcuoglu, K. Spatial transformer networks. *CoRR*, abs/1506.02025, 2015. URL http://arxiv.org/abs/1506.02025.

Kingma, D. P. and Ba, J. Adam: A method for stochastic optimization, 2017.

Kingma, D. P. and Welling, M. Auto-encoding variational bayes. *arXiv preprint arXiv:1312.6114*, 2013.

Koneripalli, K., Lohit, S., Anirudh, R., and Turaga, P. Rate-invariant autoencoding of time-series. In *ICASSP 2020 - 2020 IEEE International Conference on Acoustics, Speech and Signal Processing (ICASSP)*, pp. 3732–3736, 2020. doi: 10.1109/ICASSP40776.2020.9053983.

Kosiorek, A. R., Sabour, S., Teh, Y. W., and Hinton, G. E. Stacked capsule autoencoders, 2019.

Larochelle, H., Erhan, D., Courville, A., Bergstra, J., and Bengio, Y. An empirical evaluation of deep architectures on problems with many factors of variation. In *Proceedings of the 24th international conference on Machine learning*, pp. 473–480, 2007.

LeCun, Y., Bottou, L., Bengio, Y., and Haffner, P. Gradient-based learning applied to document recognition. *Proceedings of the IEEE*, 86(11):2278–2324, 1998.

Romero, D. W. and Cordonnier, J. Group equivariant stand-alone self-attention for vision. *CoRR*, abs/2010.00977, 2020. URL https://arxiv.org/abs/2010.00977.

Romero, D. W. and Lohit, S. Learning partial equivariances from data. *Advances in Neural Information Processing Systems*, 35:36466–36478, 2022.

Romero, D. W., Bekkers, E. J., Tomczak, J. M., and Hoogendoorn, M. Attentive group equivariant convolutional networks. *CoRR*, abs/2002.03830, 2020. URL https://arxiv.org/abs/2002.03830.

Shu, Z., Sahasrabudhe, M., Güler, R. A., Samaras, D., Paragios, N., and Kokkinos, I. Deforming autoencoders: Unsupervised disentangling of shape and appearance. *CoRR*, abs/1806.06503, 2018. URL http://arxiv.org/abs/1806.06503.

Wang, Y., Zhang, J., Kan, M., Shan, S., and Chen, X. Self-supervised equivariant attention mechanism for weakly supervised semantic segmentation. *CoRR*, abs/2004.04581, 2020. URL https://arxiv.org/abs/2004.04581.

Wang, Z., Bovik, A. C., Sheikh, H. R., and Simoncelli, E. P. Image quality assessment: from error visibility to structural similarity. *IEEE transactions on image processing*, 13(4):600–612, 2004.

Weiler, M. and Cesa, G. General e(2)-equivariant steerable cnns. *CoRR*, abs/1911.08251, 2019. URL http://arxiv.org/abs/1911.08251.

Weiler, M., Geiger, M., Welling, M., Boomsma, W., and Cohen, T. 3d steerable cnns: Learning rotationally equivariant features in volumetric data. *CoRR*, abs/1807.02547, 2018. URL http://arxiv.org/abs/1807.02547.

Winter, R., Noé, F., and Clevert, D. Permutation-invariant variational autoencoder for graph-level representation learning. *CoRR*, abs/2104.09856, 2021. URL https://arxiv.org/abs/2104.09856.

Winter, R., Bertolini, M., Le, T., Noé, F., and Clevert, D.-A. Unsupervised learning of group invariant and equivariant representations. *Advances in Neural Information Processing Systems*, 35:31942–31956, 2022.

Xiao, H., Rasul, K., and Vollgraf, R. Fashion-mnist: a novel image dataset for benchmarking machine learning algorithms, 2017.

Yokota, T. and Hontani, H. Manifold modeling in quotient space: Learning an invariant mapping with decodability of image patches, 2022.

Appendix

A. Background

Groups and group actions. A group $\mathcal{G}$ is a set equipped with a closed, associative binary operation $\cdot$ such that $\mathcal{G}$ contains an identity element $e \in G$ and every element $g \in \mathcal{G}$ has an inverse $g^{-1} \in \mathcal{G}$. For a given set $\mathcal{X}$ and group $\mathcal{G}$, the (left) group action of $\mathcal{G}$ on $\mathcal{X}$ is a map $\rho : \mathcal{G} \times \mathcal{X} \to \mathcal{X}$ that preserves the group structure. Intuitively, it describes how set elements transform by group elements.

Group representations. In this work, we focus on cases where $\mathcal{X}$ is a vector space. In such scenarios, the group acts on it by means of *group representations*. Specifically, a representation of $\mathcal{G}$ is a function $\rho_{\mathcal{X}} : \mathcal{G} \to \mathrm{GL}(\mathcal{X})$ that maps each group element to an invertible $\mathrm{n}\times\mathrm{n}$ matrix from the *general linear group* $\mathrm{GL}(\mathcal{X})$, where n is the dimension of the vector space $\mathcal{X}$. We consider our datasets to be of the form $\mathcal{X}=\{f \,|\, f : \mathcal{V} \to \mathcal{W}\}$ where $\mathcal{V}$ and $\mathcal{W}$ are vector spaces. For instance, an RGB image can be interpreted as a function $f : \mathbb{R}^2 \to \mathbb{R}^3$ that maps each pixel location to a three-channel intensity value. Following this definition, a group element acts in a data sample as:

$$[\rho_{\mathcal{X}}(g)f](x) \equiv \rho_{\mathcal{W}}(g)f\left(\rho_{\mathcal{V}}(g^{-1})x\right). \tag{9}$$

Throughout this paper, when we refer to representations $\rho_{\mathcal{X}}$ on $\mathcal{X}$, it is understood that we are implicitly referring to the previous equation to understand the transformation of each component.

Orbits. A central concept in our study is the orbit of x, defined as $\mathcal{O}_x=\{\rho_{\mathcal{X}}(g)x\}_{g\in\mathcal{G}}$. The orbit of x captures all possible transformations of x resulting from the action of all elements of $\mathcal{G}$.

Equivalence classes and quotient sets. Our analysis strongly relies on the definition of equivalence classes and their quotient sets. Let $\sim$ be an equivalence relation on $\mathcal{X}$ and consider the *equivalence classes* $[x]=\{y \in \mathcal{X},\ \text{s.t. } x \sim y\}$ of $\mathcal{X}$. The quotient set $\mathcal{X}/\sim$ is defined as the collection of all equivalent classes in $\mathcal{X}$ under the relation $\sim$.

Group equivariance and group invariance. A map $h : \mathcal{V} \to \mathcal{W}$ is $\mathcal{G}$-equivariant with respect to the representations $\rho_{\mathcal{V}}, \rho_{\mathcal{W}}$ if $h(\rho_{\mathcal{V}}(g)x) = \rho_{\mathcal{W}}(g)h(x)\ \forall g \in \mathcal{G}, \forall x \in \mathcal{X}$. In the context of neural networks, G-CNNs (Cohen & Welling, 2016) are designed to be $\mathcal{G}$-equivariant by using only $\mathcal{G}$-equivariant layers in their constructions. This ensures that applying a transformation $g \in \mathcal{G}$ before or after a layer yields the same result. Analogously, a map h is $\mathcal{G}$-invariant with respect to $\rho_{\mathcal{V}}$ if $h(\rho_{\mathcal{V}}(g)x)=h(x)\ \forall g \in \mathcal{G}, \forall x \in \mathcal{X}$. That is, if $\mathcal{G}$-transformations of the input yield the same result.

B. Proofs

Proposition B.1. *Consider a $\mathcal{G}$-invariant autoencoder $\delta \circ \eta$ and a group action estimator ψ. Under the assumption of uniformity of symmetries in $\mathcal{X}$, the following statements are equivalent:*

(i) $\psi\left(c_{[x]}\right)=e\ \forall [x] \in \mathcal{X}/\sim_{\mathcal{G}}$.

(ii) $\forall [x] \in \mathcal{X}/\sim_{\mathcal{G}}$, *the canonical representation of any $s \in [x]$ is its center of symmetry $c_{[x]}$.*

(iii) $\forall [x] \in \mathcal{X}/\sim_{\mathcal{G}}$, *it holds that $\psi([x]) = \mathcal{S}_{\theta_{[x]}}$.*

Proof. Let us prove the proposition by proving *(i)* $\Longleftrightarrow$ *(ii)* and *(i)* $\Longleftrightarrow$ *(iii)*.

(i) $\Longrightarrow$ *(ii)* Let $[x] \in \mathcal{X}/\sim_{\mathcal{G}}$. Because of uniformity of symmetries, we can write the elements of $[x]$ as $s = \rho_{\mathcal{X}}(g)c_{[x]} \in [x]$, where $g \in \mathcal{S}_{\theta_{[x]}}$. We want to prove that its canonical representation is the center of symmetry of the class, $c_{[x]}$. The canonical representation of s is given by

$$\hat{s} = \delta(\eta(s)) = \delta(\eta(\rho_{\mathcal{X}}(g)c_{[x]})) \overset{\eta\ \ G-inv}{\overset{\uparrow}{=}} \delta(\eta(c_{[x]})) \tag{10}$$

Now let us calculate the canonical representation of the center of symmetry. Because ψ is suitable, we know that

$$\rho_{\mathcal{X}}(\psi(x))\,\delta(\eta(x)) = x \quad \forall x \in X \tag{11}$$

In particular,

$$\rho_X(\psi(c_{[x]}))\,\delta(\eta(c_{[x]})) = c_{[x]} \tag{12}$$

Expanding the left-hand side of the previous equation, we get

$$\rho_{\mathcal{X}}(\psi(c_{[x]}))\,\delta(\eta(c_{[x]})) \overset{\psi(c_{[x]})=e \;\; \forall c_{[x]}\in\mathcal{X}/\sim_{\mathcal{G}}}{=} \delta(\eta(c_{[x]})) \tag{13}$$

and joining equation 10, equation 12 and equation 13 we get

$$\hat{s} = \delta(\eta(c_{[x]})) = c_{[x]} \tag{14}$$

as we wanted to show.

(ii) $\Longrightarrow$ *(i)* Let us assume that $\hat{s} = \delta(\eta(s)) = c_{[x]} \;\; \forall s \in [x] \; \forall [x] \in \mathcal{X}/\sim_{\mathcal{G}}$. Let $s \in [x]$. Because ψ is suitable, it holds that

$$s = \rho_{\mathcal{X}}(\psi(s))\delta(\eta(s)) \underset{\delta(\eta(s))=c_{[x]}}{=} \rho_{\mathcal{X}}(\psi(s))c_{[x]} \tag{15}$$

In particular, for $s = c_{[x]}$

$$c_{[x]} = \rho_{\mathcal{X}}(\psi(c_{[x]}))c_{[x]} \iff \psi(c_{[x]}) = e \tag{16}$$

as we wanted to prove.

(i) $\Longrightarrow$ *(iii)* Suppose that $\psi(c_{[x]}) = e \; \forall [x] \in \mathcal{X}/\sim_{\mathcal{G}}$. Let us prove that the group function ψ is predicting exactly the symmetries in the data, which are given by $\mathcal{S}_{\theta_{[x]}}$. Let $[x] \in X/_{\sim_{\mathcal{G}}}$. Because of uniformity of symmetries, we can write the elements of $[x]$ as $s = \rho_{\mathcal{X}}(g)c_{[x]} \in [x]$, where $g \in \mathcal{S}_{\theta_{[x]}}$. Therefore,

$$\psi(s) = \psi(\rho_{\mathcal{X}}(g)c_{[x]}) \overset{\psi \;\; G-equiv}{=} g \cdot \psi(c_{[x]}) \underset{\psi(c_{[x]})=e \;\; \forall c_{[x]}\in\mathcal{X}/\sim_{\mathcal{G}}}{=} g \in \mathcal{S}_{\theta_{[x]}} \tag{17}$$

This is, the transformations predicted by ψ on $[x]$ are the elements of $\mathcal{S}_{\theta_{[x]}}$ i.e. the symmetry distribution of $[x]$ (and *vice versa*), as we wanted to prove.

(iii) $\Longrightarrow$ *(i)* Suppose that the transformations in $\psi([x])$ are those in the data, $\mathcal{S}_{\theta_{[x]}}$. Let us prove by contradiction that $\psi(c_{[x]}) = e \; \forall [x] \in \mathcal{X}/\sim_{\mathcal{G}}$. Therefore, suppose that exists a $[x]_0 \in \mathcal{X}/\sim_{\mathcal{G}} \;\; s.t. \;\; \psi(c_{[x]_0}) \neq e$. Let $\mathcal{S}_{\theta_{[x]_0}}$ its symmetry distribution in the data.

Case 1. $\psi(c_{[x]_0}) = g_0 \notin \mathcal{S}_{\theta_{[x]_0}}$

It is clear that $\psi(c_{[x]_0})$ can not take the value of an element outside of the subset $\mathcal{S}_{\theta_{[x]_0}}$, as then we would have found a class $[x]_0$ with an element $c_{[x]_0} \in [x]_0$ whose image by ψ is not a transformation with angle in $[-\theta_0, \theta_0]$, which is a contradiction with $\psi([x]) = \mathcal{S}_{\theta_{[x]}}$ for all $[x] \in \mathcal{X}/\sim_{\mathcal{G}}$.

Case 2. $\psi(c_{[x]_0}) = g_0 \in \mathcal{S}_{\theta_{[x]_0}}, \;\; g_0 \neq e$

Consider an element of the class $s \in [x]_0$. Because of uniformity of symmetries, we can write the elements of $[x]_0$ as $s = \rho_{\mathcal{X}}(g)c_{[x]_0} \in [x]_0$, where $g \in \mathcal{S}_{\theta_{[x]_0}}$. Then,

$$\psi(s) = \psi(\rho_{\mathcal{X}}(g)c_{[x]_0}) \overset{\psi \;\; G-equiv}{=} g \cdot \psi(c_{[x]_0}) \underset{\psi(c_{[x]_0})=g_0\in\mathcal{S}_{\theta_{[x]_0}}}{=} g \cdot g_0 \tag{18}$$

Now consider the elements $s_l, s_u \in [x]_0$ that are at the lower and upper bound respectively of the uniform symmetry of $[x]_0$. Then, $s_l = \rho_{\mathcal{X}}(g_{-\theta_0})c_{[x]_0}$ and $s_u = \rho_{\mathcal{X}}(g_{\theta_0})c_{[x]_0}$ where $g_{-\theta_0}, g_{\theta_0} \in \mathcal{S}_{\theta_{[x]_0}}$ are the transformations whose rotation angles are $-\theta_0$ and θ_0 respectively. Consider their images by ψ as given by equation 18

$$\psi(s_l) = g_{-\theta_0} \cdot g_0, \quad \psi(s_u) = g_{\theta_0} \cdot g_0 \tag{19}$$

Because $g_0 \neq e$, then $g_0 = g_\alpha$ for some angle α that is strictly positive or strictly negative. If $\alpha > 0$, then $\psi(s_u) = g_{\theta_0} \cdot g_\alpha = g_{\theta_0+\alpha}$ which is not in $\mathcal{S}_{\theta_{[x]_0}}$. Similarly, if $\alpha < 0$ then $\psi(s_l) = g_{-\theta_0+\alpha} \notin \mathcal{S}_{\theta_{[x]_0}}$. In any case, we found an element of $[x]_0$ whose image by ψ is a transformation with rotation angle not in $[-\theta_0, \theta_0]$, which is a contradiction with $\psi([x]) = \mathcal{S}_{\theta_{[x]}}$ for all $[x] \in \mathcal{X}/\sim_{\mathcal{G}}$.

Therefore, $\psi(c_{[x]}) = e \ \forall [x] \in X/_{\sim_{\mathcal{G}}}$ as we wanted to show. □

Proposition B.2. *Consider a $\mathcal{G}$-invariant autoencoder $\delta \circ \eta$ and a group action estimator ψ. Under Gaussian symmetries in $\mathcal{X}$, the following statements are equivalent:*

(i) $\psi\left(c_{[x]}\right) = e \ \forall [x] \in \mathcal{X}/\sim_{\mathcal{G}}$.

(ii) $\forall [x] \in \mathcal{X}/\sim_{\mathcal{G}}$, *the canonical representation of any* $s \in [x]$ *is its center of symmetry* $c_{[x]}$.

(iii) $\forall [x] \in \mathcal{X}/\sim_{\mathcal{G}}$, *it holds that* $\psi\left([x]\right) = \mathcal{S}_{\sigma_{[x]}}$.

Remark B.3. Note that because the angles in $\mathcal{S}_{\sigma_{[x]}}$ are sampled from a Gaussian distribution $N(0, \sigma_{[x]})$, the set $\mathcal{S}_{\sigma_{[x]}}$ is not guaranteed to contain the identity element, corresponding to exactly $0°$ in the Gaussian distribution sample $S \sim N(0, \sigma_{[x]})$. For the sake of simplicity, we assume $e \in \mathcal{S}_{\sigma_{[x]}}$. In practice, this assumption does not present a problem, as the objective $\mathcal{L}_2$ ensures convergence of the canonical representation to the center of the Gaussian distribution (see Appendix B.1). Additionally, we also assume that the samples from the $N(0, \sigma_{[x]})$ are not (by chance) degenerate ($\mathcal{S}_{\sigma_{[x]}} = \{e\}$), or cyclic ($\mathcal{S}_{\sigma_{[x]}} = C_n$), case whose proof is covered in Prop 3.3.

Proof. Let us prove the proposition by proving *(i)* $\Longleftrightarrow$ *(ii)* and *(i)* $\Longleftrightarrow$ *(iii)*.

(i) $\Longrightarrow$ *(ii)*, *(ii)* $\Longrightarrow$ *(i)*, *(i)* $\Longrightarrow$ *(iii)* Same as Prop. 3.1 but for $\theta_{[x]} = \sigma_{[x]}$ and substituting the uniformity of symmetries condition by Gaussian symmetries condition.

(iii) $\Longrightarrow$ *(i)* Suppose that the transformations in $\psi([x])$ are those in the data, $\mathcal{S}_{\sigma_{[x]}}$. Let us prove by contradiction that $\psi(c_{[x]}) = e \ \forall [x] \in \mathcal{X}/\sim_{\mathcal{G}}$. Therefore, suppose that exists a $[x]_0 \in \mathcal{X}/\sim_{\mathcal{G}} \ \ s.t. \ \ \psi(c_{[x]_0}) \neq e$. Let $\mathcal{S}_{\sigma_{[x]_0}}$ its symmetry distribution in the data.

Case 1. $\psi(c_{[x]_0}) = g_0 \notin \mathcal{S}_{\sigma_{[x]_0}}$

It is clear that $\psi(c_{[x]_0})$ can not take the value of an element outside of the subset $\mathcal{S}_{\sigma_{[x]_0}}$, as then we would have found a class $[x]_0$ with an element $c_{[x]_0} \in [x]_0$ whose image by ψ is not a transformation with angle in $S \sim N(0, \sigma_{[x]_0})$, which is a contradiction with $\psi([x]) = \mathcal{S}_{\sigma_{[x]}}$ for all $[x] \in \mathcal{X}/\sim_{\mathcal{G}}$.

Case 2. $\psi(c_{[x]_0}) = g_0 \in \mathcal{S}_{\sigma_{[x]_0}}, \quad g_0 \neq e$

Consider an element of the class $s \in [x]_0$. Under Gaussian symmetries, we can write the elements of $[x]_0$ as $s = \rho_{\mathcal{X}}(g)c_{[x]_0} \in [x]_0$, where $g \in \mathcal{S}_{\sigma_{[x]_0}}$. Then,

$$\psi(s) = \psi(\rho_{\mathcal{X}}(g)c_{[x]_0}) \overset{\psi \ \ G\text{-}equiv}{=} g \cdot \psi(c_{[x]_0}) \underset{\psi(c_{[x]_0}) = g_0 \in \mathcal{S}_{\sigma_{[x]_0}}}{=} g \cdot g_0 \tag{20}$$

Proceeding as in Prop. 3.1, if we find an element $s \in [x]_0$ such that $\psi(s) \notin \mathcal{S}_{\sigma_{[x]_0}}$, we will have proved the result by contradiction with $\psi([x]) = \mathcal{S}_{\sigma_{[x]}}$ for all $[x] \in \mathcal{X}/\sim_{\mathcal{G}}$.

Because $g_0 \neq e$, then $g_0 = g_\alpha$ for some angle $\alpha \in S \sim N(0, \sigma_{[x]})$ that is strictly positive or strictly negative. Assume $g_0 = g_\alpha$ with $\alpha > 0$. Because the sample S is finite, there exists $u = max\{S\}$. Consider its corresponding element $s_u \in [x]_0$ w.r.t. the center of symmetry of the distribution as $s_u = \rho_\mathcal{X}(g_u)c_{[x]_0}$. By equation 20,

$$\psi(s_u) = g_u \cdot g_\alpha = g_{u+\alpha}, \tag{21}$$

where $u + \alpha > u \implies \psi(s_u) \notin \mathcal{S}_{\sigma_{[x]_0}}$ as $u = max\{S\}$, which finalizes the proof. □

Proposition B.4. *Consider a $\mathcal{G}$-invariant autoencoder $\delta \circ \eta$ and a group action estimator ψ. Under cyclic symmetries in $\mathcal{X}$, the following statements are equivalent:*

(i) $\psi\left(c_{[x]}\right) = e \ \forall [x] \in \mathcal{X}/\sim_\mathcal{G}$ *for some* $c_{[x]} \in [x]$.

(ii) $\forall [x] \in \mathcal{X}/\sim_\mathcal{G}$, *the canonical representation of any* $s \in [x]$ *is the element* $c_{[x]} \in [x]$.

(iii) $\forall [x] \in \mathcal{X}/\sim_\mathcal{G}$, *it holds that* $\psi([x]) = \mathcal{C}_{n_{[x]}}$.

Proof. The proof is immediate by following the proofs for *(i)* $\iff$ *(ii)* and *(i)* $\implies$ *(iii)* as in Prop. 3.1, by substituting the uniformity of symmetries condition by cyclic condition. *(i)* $\implies$ *(iii)* is immediate. □

B.1. Convergence of $\mathcal{L}_2$ towards the centers of symmetry

Minimizing $\mathcal{L}_2$ intuitively encourages convergence towards the centers of symmetry of both uniform and Gaussian distributions, and in general, arbitrary unimodal, symmetric distributions. Consider a class $[x] = \{\rho_\mathcal{X}(g)c_{[x]} \ s.t. \ g \in \mathcal{S}_{\theta_{[x]}}\}$ and the proposed minimization objective

$$\mathcal{L} = \mathcal{L}_1 + \mathcal{L}_2 = d_1\left(\rho_\mathcal{X}(\psi(x))\,\delta(\eta(x)), x\right) + d_2\left(\psi(x), e\right). \tag{22}$$

We know that the standard IE-AE loss $\mathcal{L}_1$ results in an arbitrary element of the orbit of x chosen as canonical, that is, $\psi(o_x) = e$ for some $o_x \in \mathcal{O}_x$.

Now, focusing on minimizing the $\mathcal{L}_2 = d_2\left(\psi(x), e\right)$ loss in our model, it seems to merely ensure that the canonical representation for an IE-AE is an actual member of the equivalence class, meaning $\psi(s) = e$ for some $s \in [x]$. However, it can be shown that the specific member within this range that minimizes the $\mathcal{L}_2$ loss is in fact the center of this symmetry. To build on this intuition, consider the uniform case, and define the distance between two group elements g_α, g_β with rotation angles $\alpha, \beta \in [-180, 180]$ as $d_2(g_\alpha, g_\beta) = |\alpha - \beta|$. The objective $\mathcal{L}_2$ ensures that the canonical element is some element of the class i.e. $\psi(s_0) = e$ for some $s_0 \in [x]$ with rotation angle $\alpha_0 \in [-\theta, \theta]$. We will show that this element is precisely the center of symmetry $c_{[x]}$, i.e. the one corresponding to a zero degree rotation in $[-\theta, \theta]$. Let us calculate the expected value of $\mathcal{L}_2$ for the elements in the class:

$$\begin{aligned}
&\mathbb{E}_{s\in[x]}(\mathcal{L}_2(s)) = \mathbb{E}_{s\in[x]} d_2(\psi(s), e) = \\
&= \frac{1}{2\theta}\int_{-\theta}^{\theta} d_2(g_\alpha, e)\, d\alpha = \frac{1}{2\theta}\int_{-\theta}^{\theta} d_2(g_\alpha, \psi(s_0))\, d\alpha = \frac{1}{2\theta}\int_{-\theta}^{\theta} d_2(g_\alpha, g_{\alpha_0})\, d\alpha = \\
&= \frac{1}{2\theta}\int_{-\theta}^{\theta} |\alpha - \alpha_0|\, d\alpha = \frac{1}{2\theta}\left(\int_{-\theta}^{\alpha_0} -\alpha + \alpha_0\, d\alpha + \int_{\alpha_0}^{\theta} \alpha - \alpha_0\, d\alpha\right) = \\
&= \frac{1}{2\theta}\left(\alpha_0^2 + \theta^2\right)
\end{aligned} \tag{23}$$

This is minimized when $\alpha_0 = 0$, i.e. when the choice of the canonical is $\psi(g_0) = \psi(c_{[x]}) = e$, the center of symmetry. Therefore, minimizing $\mathcal{L}_2$ effectively guarantees solutions that comply with Proposition 3.1.

The previous derivation can be similarly extended to the center of symmetry of Gaussian symmetries. In this context, we substitute the integral ($\int$) with a summation ($\sum$), considering that we are dealing with finite samples, to arrive to an equivalent understanding. Furthermore, this reasoning can be applied in general to arbitrary unimodal, symmetric distributions, that is, any distribution that shows a center of symmetry.

As for the case of cyclic distributions, the result is straightforward, as the requirement of a center of symmetry is relaxed to any element of the class $c_{[x]} \in [x]$ (see Prop. 3.3 *(i)*), which is already sufficient to capture a cyclic distribution, given its inherently symmetric structure. The condition $c_{[x]} \in [x]$ is inherently satisfied by the $\mathcal{L}_2$ minimization, which obviates the need for further derivations.

C. Pseudo-label Estimators

Uniform Distributions For simplicity in notation, we use the notation $\psi(\mathcal{N}_k(x))$ both to denote the set of group elements predicted by ψ in the subset $\mathcal{N}_k(x)$ and their rotation angles as a subset of $[-180°, 180°]$. Let's consider the distribution of these rotation angles, $\psi(\mathcal{N}_k(x))$, and its absolute value form $|\psi(\mathcal{N}_k(x))|$.

The decision to use the method of moments estimator for generating pseudo-labels is motivated by its robustness to outliers, compared to other potential estimators. Let's consider the alternative of a maximum likelihood estimator (MLE) for the distribution $\psi(\mathcal{N}_k(x))$, which is the maximum in $\psi(\mathcal{N}_k(x))$. This approach is particularly sensitive to outliers. For example, if any element in $\mathcal{N}_k(x)$ has an erroneously predicted high rotation angle, the pseudo-label for x will be disproportionately influenced by this outlier. In contrast, the method of moments estimator for the $|\psi(\mathcal{N}_k(x))|$ distribution, which we employ, calculates the pseudo-label as two times the mean of all angles in $|\psi(\mathcal{N}_k(x))|$. This averaging effect mitigates the impact of any occasional anomalous angles, as these outliers are diluted when calculating the mean. Therefore, the method of moments approach offers a more stable and representative estimate.

Following this reasoning, we estimate the pseudo-labels as E=$2 \cdot \overline{|\psi(\mathcal{N}_k(x))|}$, where $\overline{|\psi(\mathcal{N}_k(x))|}$ corresponds to the mean rotation angle in $|\psi(\mathcal{N}_k(x))|$. Additionally, when calculating $\mathcal{N}_k(x)$, we exclude the element x from being its own nearest neighbour to avoid potential biases in the calculation of the pseudo-labels. Finally, we consider the optional implementation of an outlier detection method for $|\psi(\mathcal{N}_k(x))|$, such as the Interquartile Range (IQR) method. In our approach, rotations that are more than two standard deviations away from the mean are excluded, aiming to produce more consistent and stable pseudo-labels.

Gaussian Distributions In the Gaussian case, $|\psi(\mathcal{N}_k(x))|$ follows a half-normal distribution. The standard deviation from the original normal distribution can be computed as E=$\frac{\sigma}{1-2/\pi}$ where σ is the standard deviation of the sample $\psi(\mathcal{N}_k(x))$.

Cyclic Distributions We can estimate the cyclic group to which the distribution $\psi(\mathcal{N}_k(x))$ corresponds by calculating the Kullback-Leibler divergence from $\psi(\mathcal{N}_k(x))$ to f_n, where f_n is the equivalent of $\mathcal{C}_n$ as a continuous distribution defined in $[-180°, 180°]$.

To determine the cyclic group $\mathcal{C}_n$ that best represents the distribution $\psi(\mathcal{N}_k(x))$, we compute the Kullback-Leibler (KL) divergence between $\psi(\mathcal{N}_k(x))$ and a continuous distribution f_n, defined as the continuous counterpart of the discrete cyclic group $\mathcal{C}_n$ over the interval $[-180°, 180°]$. Specifically, f_n is constructed as a uniform distribution over n equidistant points within this interval, reflecting the rotational symmetries in $\mathcal{C}_n$:

$$f_n(\alpha) = \frac{1}{n} \sum_{i=1}^{n} \delta(\alpha - \alpha_i), \tag{24}$$

where δ is the Dirac delta function, α represents the angle in degrees, and α_i are the n equidistant angles (symmetry positions) in [-180,180] corresponding to $\mathcal{C}_n$. The KL divergence between the empirical distribution $\psi(\mathcal{N}_k(x))$ and f_n is then calculated to quantify the similarity between them. This divergence is given by:

$$D_{\mathrm{KL}}(P \| Q_n) = \sum_i P(i) \log\left(\frac{P(i)}{Q_n(i)}\right) \tag{25}$$

where P is the normalized histogram of $\psi(\mathcal{N}_k(x))$ over 360 bins and Q_n is the discretized version of f_n over the same bins as P.

This KL divergence metric allows us to estimate the most likely cyclic group $\mathcal{C}_n$ that the distribution $\psi(\mathcal{N}_k(x))$ aligns with, providing a measure of how well the empirical distribution matches the expected rotational symmetries of $\mathcal{C}_n$. Therefore, the pseudo-label of x is calculated as:

$$\hat{\theta}_x = argmin_{n \in \mathbb{N}} D_{\mathrm{KL}}(P \| Q_n) \tag{26}$$

Practically, our comparisons are limited to a finite range of cyclic groups. We consider the range from $\mathcal{C}_1$ to $\mathcal{C}_8$ to be enough for practical applications, although the number of cyclic groups to consider can be increased at the cost of compute. Finally, note that in order to be consistent with the notation established throughout the paper, we used the notation $\hat{\theta}_x$ for the pseudo-labels, although the cyclic group pseudo-labels $\hat{\theta}_x$ belong to $\mathbb{N}$ and represent the corresponding cyclic group, rather than a continuous value as in the uniform case.

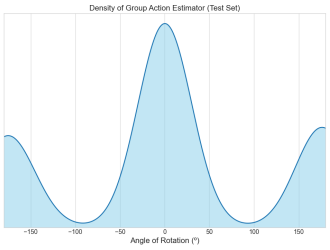

(a) Density of ψ for digit 3 in MNISTC2-C4.

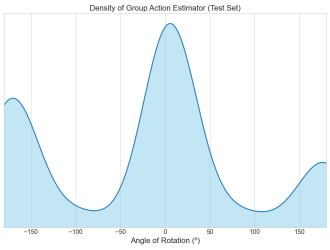

(b) Density of ψ for digit 4 in MNISTC2-C4.

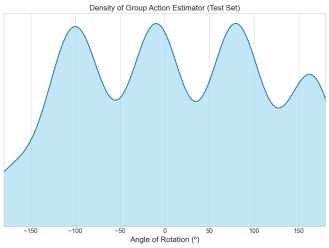

(c) Density of ψ for digit 5 in MNISTC2-C4.

Figure 6. Density of ψ for MNISTC2-C4 in different classes. It is important to note a visualization artifact near the x-axis limits at $-180°$ and $180°$. Due to these points lying exactly on the circular boundary (the break point of the circle S^1), the peaks appear artificially lower than their actual values in the plot. This apparent reduction in density is a result of projecting the circular distribution onto a straight line for visualization. In reality, both $\mathcal{C}_2$ and $\mathcal{C}_4$ distributions exhibit a single, prominent peak at the point where $-180°$ and $180°$ converge on the circle.

D. Additional experimental information

D.1. Model configuration and training

In all our experiments, the encoder η, the network Θ, and the constrained group function $\overline{\psi}$ are built using SO(2) equivariant/invariant networks from Weiler & Cesa (2019). We maintained consistent network sizes across all experiments. The encoder architecture comprises seven SO(2) invariant convolutional layers with feature maps increasing from 128 in the first layer to 256, and 200 feature maps at the output. Each convolutional layer is followed by a batch normalization and a ReLU activation, except the final block which employs global average pooling. The $\overline{\psi}$ function resembles the encoder η but employing SO(2)-equivariant convolutional layers with feature maps ranging from 64 to 128. Similarly, the Θ network resembles the group function $\overline{\psi}$ with 64 initial feature maps for continuous distributions, and 32 for cyclic distributions, followed by three fully-connected layers with ReLU activations. Lastly, the decoder δ is designed with conventional convolutional and upsampling layers to inversely replicate the η encoder's structure. Note that the Θ network has a single neuron output for the uniform and Gaussian distributions case, while n for the cyclic case, where n is the number of cyclic distributions that we want to compare to. In our case, we use $n = 8$, but arbitrarily higher order groups can be considered.

The number of neighbors k for the Θ network varies with each experiment: 45 for uniform and Gaussian distributions, and 150 for cyclic. Cyclic group estimations require more neighbors as this computation relies on the comparison between distributions via the KL divergence, which demands a higher number of points to be reliable. In contrast, continuous distributions allow fewer neighbors, as their pseudo-labels are derived through parameter estimation, typically reliable with k over 30. Selecting the number of neighbors involves balancing more accurate estimations against the risk of incorporating elements with differing symmetry distributions, which could destabilize the pseudo-label estimations.

During the pre-training phase and self-supervised training, the models undergo 400 and 150 epochs respectively. Both the constrained IE-AE and the Θ network use the Adam (Kingma & Ba, 2017) optimizer, combined with a cosine scheduler with 5 warm-up epochs. The learning rates are set at 0.01 for the IE-AE and 0.001 for the Θ network. Additionally, the $\mathcal{L}_2$ loss is assigned a weight of 0.03125 to maintain balanced optimization in conjunction with the $\mathcal{L}_1$ loss.

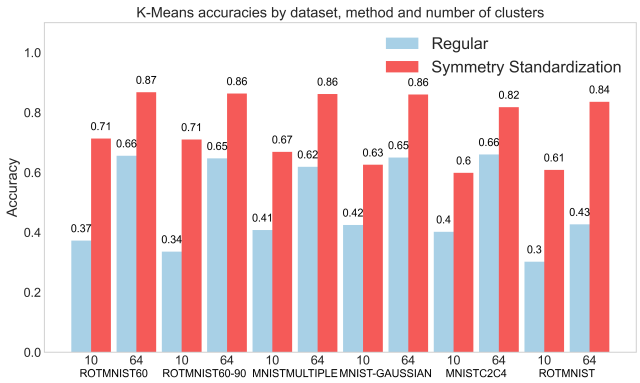

Figure 7. Results for K-Means in MNIST variants.

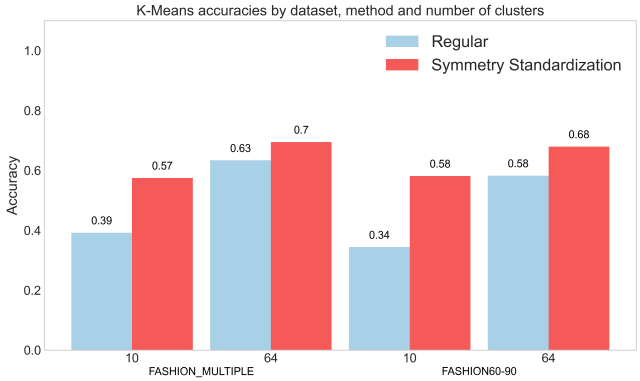

Figure 8. Results for K-Means in FashionMNIST variants.

D.2. Out-of-distribution and Symmetry Standardization Experiments

For the out-of-distribution symmetries detector, we use the models obtained after training in the datasets with partial symmetries. No further training is necessary, as the classifier relies on the generalization capabilities of the Θ function, already trained. During inference, an input is classified to be out of the distribution of the training dataset when its predicted group action angle $\psi(x)$ is outside of the symmetry distribution predicted by Θ. In the case of cyclic distributions, because the predicted distributions in Θ are discrete, we consider that an input is out-of-distribution if it deviates more than 5° from an element of $\mathcal{C}_n$.

For the symmetry standardization, baseline supervised and unsupervised models are first trained and tested in the datasets variants to create the "no symmetry standardization" results. Similarly, the "symmetry standardization results" are created using the symmetry standardized training and test datasets obtained after training our model. K-Means is trained with different number of clusters as shown in Fig. 7 for MNIST and Fig. 8. Classification of each of K-Means is calculated based on class majority of that cluster. ResNet-18 is trained from scratch for 100 epochs, using an Adam optimizer with learning rate 0.001. Finally, a KNN supervised classifier with 5 neighbors is trained on the $\mathcal{G}$−invariant embeddings of the standard, pre-trained IE-AEs in each of the datasets. Test accuracy is computed similarly, by first computing the IE-AE embeddings and then predicting with the trained KNN.

Table 3. Mean predicted level of symmetry for symmetry prediction in test set for each MNIST dataset.

CLASS	MNISTROT60		MNISTROT60-90		MNISTMULTIPLE		MNIST		MNISTROT		MNISTGAUSSIAN	
	θ	$\overline{\Theta}$	θ	$\overline{\Theta}$	θ	$\overline{\Theta}$	θ	$\overline{\Theta}$	θ	$\overline{\Theta}$	σ	$\overline{\Theta}$
0	60º	61.04º	60º	65.18º	0º	8.66º	0º	8.22º	180º	177.29º	0º	15.23º
1	60º	63.14º	60º	63.18º	18º	4.87º	0º	1.79º	180º	179.27º	9º	8.06º
2	60º	61.33º	60º	67.66º	36º	35.26º	0º	6.25º	180º	178.23º	18º	23.69º
3	60º	60.45º	60º	66.30º	54º	58.85º	0º	4.14º	180º	179.93º	27º	27.25º
4	60º	59.44º	60º	64.90º	72º	75.70º	0º	6.57º	180º	181.55º	36º	38.89º
5	60º	63.33º	90º	85.46º	90º	88.48º	0º	8.22º	180º	184.55º	45º	42.46º
6	60º	60.64º	90º	85.05º	108º	106.83º	0º	6.68º	180º	178.53º	54º	50.35º
7	60º	60.60º	90º	84.88º	126º	117.91º	0º	3.12º	180º	181.33º	63º	53.02º
8	60º	59.28º	90º	82.78º	144º	134.08º	0º	4.14º	180º	175.30º	72º	59.34º
9	60º	61.55º	90º	83.66º	162º	156.38º	0º	4.48º	180º	179.65º	81º	64.70º

Table 4. Mean Absolute Error of symmetry level prediction in the test set for each MNIST dataset.

CLASS	MNISTROT60		MNISTROT60-90		MNISTMULTIPLE		MNIST		MNISTROT	
	θ	MAE	θ	MAE	θ	MAE	θ	MAE	θ	MAE
0	60º	4.92	60º	5.09	0º	25.62	0º	5.43	180º	8.38
1	60º	9.51	60º	7.96	18º	8.19	0º	0.53	180º	6.64
2	60º	4.00	60º	6.24	36º	11.63	0º	2.75	180º	7.94
3	60º	3.72	60º	5.78	54º	8.88	0º	1.56	180º	7.98
4	60º	4.68	60º	6.76	72º	12.51	0º	2.20	180º	9.00
5	60º	5.94	90º	5.43	90º	10.43	0º	1.98	180º	7.98
6	60º	3.86	90º	5.09	108º	11.17	0º	3.16	180º	9.27
7	60º	3.62	90º	7.87	126º	14.95	0º	1.33	180º	8.90
8	60º	4.19	90º	7.27	144º	14.48	0º	1.46	180º	11.78
9	60º	4.67	90º	5.81	162º	18.46	0º	1.41	180º	10.05

Table 5. Mean predicted level of symmetry for symmetry prediction in the test set for each FashionMNIST dataset.

CLASS	FASHION60-90		FASHIONMULTIPLE	
	θ	$\overline{\Theta}$	θ	$\overline{\Theta}$
0	60º	68.92º	0º	17.95º
1	60º	64.27º	18º	20.79º
2	60º	66.91º	36º	54.39º
3	60º	64.76º	54º	60.46º
4	60º	65.95º	72º	73.16º
5	90º	94.23º	90º	112.30º
6	90º	77.27º	108º	77.66º
7	90º	97.05º	126º	152.03º
8	90º	129.00º	144º	153.15º
9	90º	89.40º	162º	164.94º

Table 6. Mean predicted level of symmetry for symmetry prediction in the test set for each FashionMNIST dataset.

Class	FASHION60-90		FASHIONMULTIPLE	
	θ	MAE	θ	MAE
0	60º	11.63	0º	18.21
1	60º	12.18	18º	5.22
2	60º	10.82	36º	19.98
3	60º	9.85	54º	15.95
4	60º	11.03	72º	11.64
5	90º	7.62	90º	24.98
6	90º	15.87	108º	32.94
7	90º	9.71	126º	26.91
8	90º	42.73	144º	31.02
9	90º	5.32	162º	11.66